ELSEVIER

Surface Science 319 (1994) 277–286

surface science

Pseudomorphic growth of thin Cu films on Pd(110)

Elmar Hahn, Elisabeth Kampshoff, Alexander Fricke, Jean-Pierre Bucher, Klaus Kern *

Institut de Physique Expérimentale, EPF Lausanne, CH-1015 Lausanne, Switzerland

Received 21 March 1994; accepted for publication 2 August 1994

Abstract

The growth of thin Cu films on Pd(110) has been studied by variable temperature scanning tunneling microscopy in the temperature range $250 \leq T_s \leq 900$ K. Cu adatom diffusion on the substrate is highly anisotropic and determines the submonolayer Cu island shapes. This leads at low deposition temperatures ($T_s \leq 300$ K) and low Cu coverages ($\theta < 0.1$ ML) to the formation of monatomic Cu chains oriented along [1$\bar{1}$0]. At higher coverages and/or deposition temperatures two-dimensional (2D) islands of anisotropic shape grow. At 300 K the 2D Cu-islands are arranged in a semi-ordered striped domain structure along the [001] direction. In the Cu multilayer range, the film growth mode can be varied through deposition temperature control. Microrough Cu films consisting of small 3D clusters grow below 400 K. Between 400 and about 550 K, Stranski–Krastanov growth with a critical thickness of one monolayer takes place. At 550 K, a transition to a layer-by-layer step-flow mode occurs. Flat Cu multilayers are found to be (1×1) pseudomorphic up to a critical thickness of 5 ML. Thicker films partially relieve their misfit strain through uniaxial relaxation into a (29×1) high-order commensurate structure. At temperatures above 750 K, we observe CuPd intermixing.

1. Introduction

The study of epitaxial growth of thin films vapor-deposited on solid substrates has a long history which has led to a generally accepted classification into three growth modes: Volmer–Weber (VW) growth, the formation of 3D islands on the substrate, Frank–van der Merwe (FM) or layer-by-layer growth and Stranski–Krastanov (SK) growth, where a change from layer-by-layer to 3D growth sets in at a critical film thickness. In the thermodynamic limit, where the film is able to reach its equilibrium configuration, FM growth is expected if the condition $\gamma_s \geq \gamma_{f,n} + \gamma_{i,n}$ is fulfilled independent of the film thickness [1], where γ_s and $\gamma_{f,n}$ are the surface free energies of substrate and film and $\gamma_{i,n}$ is the interface energy containing the thickness-dependent (n: number of layers) strain energy in the film, which is essentially determined by the structural misfit between substrate and adlayer material. If the strain energy is positive and increases with n, then at a given n_{crit} the FM condition is no longer valid and SK or VW (if $n_{crit} = 1$) growth occurs.

In most cases, thin films are grown under experimental conditions far from thermal equilibrium. Film growth and the resulting morphologies will then be governed by kinetic effects. In order to enable the often desired FM growth, interlayer mass transport must be sufficiently fast to allow atoms to leave the tops of islands or clusters as fast as they arrive. This

* Corresponding author. Fax: +41 21 693 3604.

SSDI 0039-6028(94)00474-9

is in general a delicate balance between several factors like the deposition rate, the adatom diffusion barrier, the activation barrier for an adatom to step down from the island perimeter and finally the density, size and shape of adlayer islands [2,3]. Many atomic details of the film growth have recently been revealed by spatial resolving techniques like field ion microscopy (FIM) [4] and scanning tunneling microscopy (STM) [5].

In the present article, we report on a variable temperature STM study of the growth of thin Cu films on Pd(110) in the temperature range $250 \leq T_s \leq 900$ K. Interest in this system arises from the fact that Cu-based bimetallic catalysts show superior properties in terms of reactivity, selectivity and stability in comparison to their single metal counterparts [6]. These properties can be controlled by tailoring the composition of the bimetallic surface. Cu and Pd are both catalysts for methanol synthesis [7], supported bimetallic CuPd particles have been shown to maintain a high turnover rate for CO oxidation over a much wider temperature range than the elementary catalysts alone [8].

The large negative surface energy difference between copper and palladium ($\gamma_{Cu} - \gamma_{Pd} < 0$) should favor the completion of at least the first Cu layer on Pd substrates. Indeed, despite the rather large structural misfit (7%) between both metals, Cu has been found to grow pseudomorphically on both Pd(111) [9] and Pd(100) [10,11], forming a novel bct-phase (bct – body centered tetragonal) on the latter surface. We have chosen Pd(110) as substrate because the anisotropic surface structure was expected to play an important role in the film growth process. Only a few STM studies [12–14] have dealt so far with this subject.

Our STM study clearly reveals the decisive influence of the substrate anisotropy on the film morphology of the Cu films. The effect is most pronounced in the submonolayer range, where the Cu island shapes are found to be dominated by the anisotropy of Cu adatom diffusion. We demonstrate further that the submonolayer island shapes as well as the multilayer growth mode can be tailored via careful control of the deposition temperature.

2. Experimental

The experiments were carried out in a stainless steel two-chamber UHV system (base pressure 1×10^{-10} mbar) described in detail in Ref. [15]. One chamber is equipped with instrumentation for sample preparation and control, i.e. ion gun (fixed ion en-

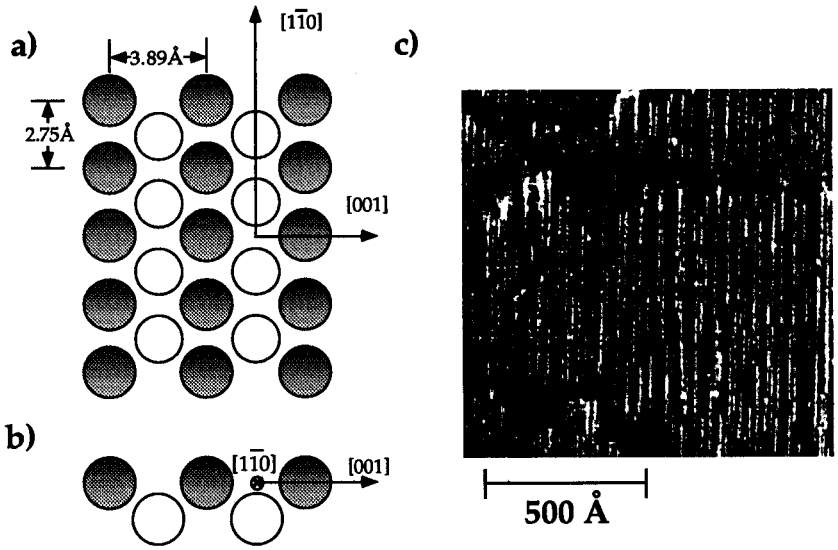

Fig. 1. Schematic (a) top and (b) side view of the Pd(110) surface. (c) 1200 Å × 1200 Å STM picture of Cu islands on Pd(110) deposited and imaged at $T_s = 265$ K, Cu coverage 0.1 ML. All STM images in this article were recorded in differential mode, which means that the derivatives of the lines of constant current were recorded.

ergy 800 eV), CMA–Auger electron spectrometer, reverse view LEED, quadrupole mass analyser and Knudsen cell for metal evaporation. By a long travel manipulator, the sample can be transferred into a second chamber, which contains a scanning tunneling microscope of the "beetle"-type [16], allowing temperature-dependent STM measurements in the range $150 \leq T_s \leq 600$ K. In addition, the apparatus is equipped with a Fourier transform infrared spectrometer and suitable optics for reflection absorption infrared spectroscopy studies.

The Pd(110) surface is unreconstructed [17] and shows a rectangular unit cell with interatomic spacings of 2.75 Å in the $[1\bar{1}0]$ direction, corresponding to the Pd lattice parameter, and 3.89 Å in the [001] direction (Fig. 1a). The crystal was prepared in UHV by repeated cycles (ca. 50 cycles in the initial preparation procedure) of Ar ion sputtering at 700 K, heating in 2×10^{-6} mbar oxygen at 620 K and subsequent annealing at 950 K. This procedure resulted in a sharp (1×1) LEED pattern with low diffuse background. Auger spectra showed no contamination of the surface (noise limit of the analyser < 0.01 ML). However a Pd Auger peak completely overlaps the characteristic carbon signal at 270 eV, thus the surface cleanliness with respect to carbon was directly verified by STM (in deliberately C-poisoned samples the carbon was found to cluster on the surface, which were imaged as bright spots by the STM). The Pd(110) surface showed an average terrace width of only 85 Å, however individual terraces up to 2000 Å wide were observed occasionally. The

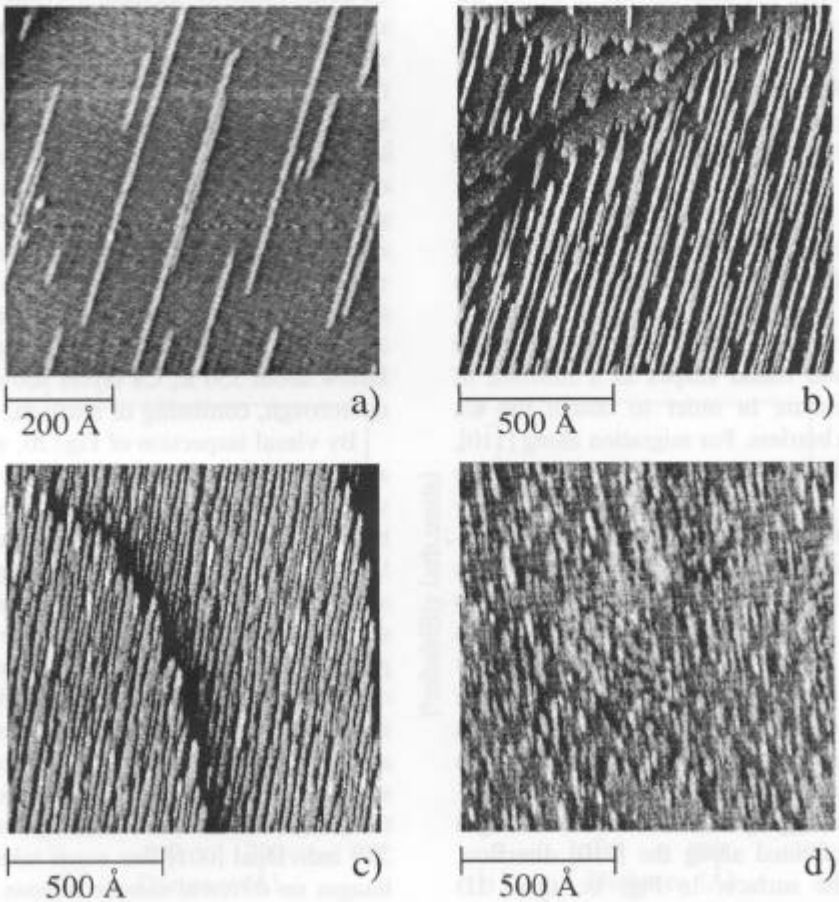

Fig. 2. Series of STM images showing the growth of Cu on Pd(110) at $T_s = 300$ K. Cu coverages (a) 0.07 ML, (b) 0.35 ML, (c) 0.7 ML, (d) 1.2 ML. All images span the size 1200 Å × 1200 Å except for (a) (size 670 Å × 670 Å).

high step density of the surface is not due to a miscut (nominally 0.2°), since up- and down-steps are present to the same extent. It is rather attributed to the low step free energy for Pd(110) [18].

Copper (purity 99.99%) was deposited by means of the Knudsen cell at a constant rate of $(1 \pm 0.05) \times 10^{-3}$ monolayers per second (1 ML = 9.35×10^{14} atoms/cm^2) at the indicated substrate temperature T_s. The surface was subsequently imaged at the same crystal temperature. Only films deposited at $T_s > 550$ K were quenched to room temperature before imaging. The STM measurements were performed in the constant current mode at 0.2–1 V positive or negative tip bias and 0.5–1.5 nA tunneling current. The Cu deposition rate was calibrated by measuring the fraction of large substrate terraces which is covered by Cu islands upon submonolayer deposition at room temperature.

3. Results and discussion

3.1. $T_s < 400$ K, the regime of diffusion-determined growth

In the Cu submonolayer range, the anisotropy of the Pd(110) surface unit cell determines the Cu adatom diffusion properties. In an earlier paper [19], we have performed a detailed analysis of the Cu island densities and island shapes as a function of deposition temperature in order to obtain the Cu adatom migration barriers. For migration along [1$\bar{1}$0], the direction of the close-packed Pd atom rows, we have measured a barrier of 0.51 eV, a substantially lower value than for migration along [001] (measured to be 0.75 eV). As a consequence of this large diffusion anisotropy, migration of Cu atoms across the close-packed Pd atom rows is completely frozen in at $T_s < 300$ K. This is demonstrated in Fig. 1c for $T_s = 265$ K: each Cu adatom which has landed on the surface migrates along [1$\bar{1}$0] until it is trapped by a substrate step edge or encounters a preexisting Cu island. Thus at low coverage ($\theta \leq 0.1$ ML for $T_s =$ 265 K) linear Cu aggregates, monatomic in width and exclusively oriented along the [1$\bar{1}$0] direction, are formed on the surface. In Fig. 1c, these 1D aggregates have an average length of 130 Å, corresponding to 50 Cu atoms arranged along [1$\bar{1}$0]. When the deposition temperature approaches 300 K, individual Cu chains can reach a length of 300 atoms (Fig. 2a; same deposition flux as in Fig. 1).

Fig. 2 displays a series of STM images characterizing the growth of a thin Cu film on Pd(110) at $T_s = 300$ K. At this temperature Cu adatom diffusion along [001] is still very slow, however the diffusion contributes to the island growth process as shown in Fig. 2b. At a coverage of 0.35 ML the Cu islands have an average width of 19 Å, corresponding to about 5 close-packed Cu rows. As indicated by a sharp (1×1) LEED pattern without any additional spots and the flat imaging by STM, the islands grow in a pseudomorphic (1×1) structure. Since the Cu lattice parameter is smaller (3.61 Å) than that of Pd, the Cu islands are considerably strained (7%) with respect to bulk Cu. The role of substrate step edges as heterogeneous nucleation centers is indicated by the Cu "fingers" growing outward from substrate steps. Increasing the coverage further to 0.7 ML (Fig. 2c), the gaps between the Cu islands are filled up, resulting in a growth of island width (about 40 Å in average) but also the onset of coalescence. At this coverage second layer nucleation is observed on top of the first layer Cu islands for the first time. The nuclation density in the second layer is much higher than on the substrate (Fig. 2d) and the diffusion anisotropy is less marked. However, second layer Cu islands are still exclusively oriented along [1$\bar{1}$0]. Below about 350 K, Cu layers above 1 ML thick are microrough, consisting of small 3D Cu clusters.

By visual inspection of Fig. 2b, a surprising detail attracts attention. While the monatomic Cu chains at very low coverages appear as randomly distributed, two-dimensional Cu chains at intermediate submonolayer coverages appear to be arranged in an at least semi-ordered striped structure, a part of the islands shows even a completely regular arrangement (lower part of Fig. 2b). To analyse the apparent mesoscopic order on a more quantitative level, histograms of the island distances along the [001] direction were evaluated. For a given Cu island, the distances to the first, second, third and all other neighbouring islands in the [001] direction have been measured. The data of 250 individual [001] line scans taken from 10 STM images on different sample regions have been compiled and are shown in histograms in Fig. 3 for coverages of 0.07 and 0.35 ML Cu. These his-

tograms can be understood as one-dimensional island–island correlation functions. The distribution for the monatomic Cu chains (Fig. 3a) shows indeed the absence of any long-range order, since all island–island distances are present with nearly equal probability (note that the scatter in the data is due to statistics). Only at the lowest distances (≤ 20 Å) a drop of the occurrence probability is noticed, which might be interpreted as a repulsive island–island interaction, giving rise to a depleted zone of some Å around a Cu chain. The distance distribution of the two-dimensional islands at a coverage of 0.35 ML, however clearly reveals the presence of some long-range order. Distinct maxima at island separations of 40, 80 and 120 Å are present. The values are multiples of the average island separation at this coverage (40 Å), showing an enhanced probability to find neighbouring islands at these particular positions. The loss of order with increasing distance from a given island resembles the typical behaviour for glasses or liquids.

Mesoscopic domain ordering was observed on Si(100) [20], on clean Pd(110) [18], on Au(111) [21] or in the system Cu(110):O [22]. Physical origins for these ordering phenomena are believed to be long range elastic and/or electrostatic interactions in the latter case [23]. The Cu islands are under considerable tensile stress due to the 7% lattice mismatch between Cu and Pd. The stressed Cu-islands relax at the boundary and exert a force on the Pd(110) substrate, which is elastically distorted. This strain relief mechanism lowers the island energy at the expense of elastic strain in the substrate. Assuming a mixed uniaxial phase of alternating stripes of Cu covered (phase A, coverage θ and width L_A) and Cu free domains (phase B, coverage 1-θ and width L_B), the energy per unit area of this structure is [23,24]

$$\Delta E = \theta \Delta E_0 + \frac{F_s}{L} - \frac{C}{L} \ln[(L/\pi a)\sin(\pi\theta)]. \quad (1)$$

Here $\Delta E_0 = E_B - E_A$ denotes the difference of the surface energies of the phases A and B, F_s is the free energy of a Cu/Pd(110) step per unit length, $L = (L_A + L_B)/2$ is the average domain width, a is the lattice constant and C is a constant determined by the elastic properties and the difference of the surface stress within the two domain types. It can be shown that for $|\Delta E_0| < C/[a \exp(F_S/C + 1)]$, a periodic domain structure is favoured. The equilibrium periodicity of this ordered striped domain phase is obtained by minimizing ΔE with respect to L at constant coverage θ:

$$D = \pi a \csc(\pi\Theta) \exp[(F_s/C) + 1], \quad (2)$$

with $D = 2L$. Recently it has been shown [25] that there should exist a firm relation between this do-

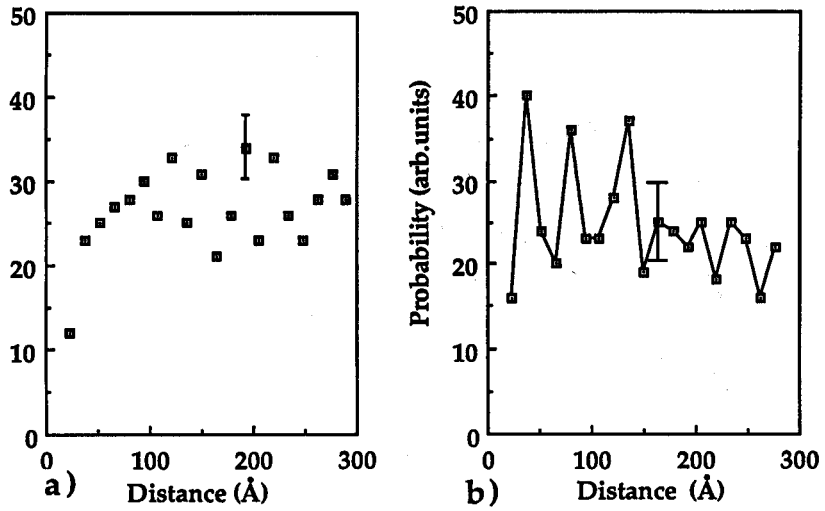

Fig. 3. Histograms showing island–island separations along the [001] direction upon Cu deposition at 300 K for (a) $\theta = 0.07$ ML, (b) $\theta = 0.35$ ML.

main periodicity D at intermediate coverages θ and the width of a single island at low island concentration $L_0 = L_A(\theta \to 0)$, independent of the actual system (e.g. the constants F_s, C and a). This size ratio should be in the interval $1/4 < L_0/D < 1/3$.

Obviously this is not consistent with our case. In the limit $\theta \to 0$, the islands are monatomic in width ($L_0 = 2.75$ Å) while the average separation at medium coverage ($\theta = 0.35$) is $D = 40$ Å, giving rise to a size ratio $L_0/D = 1/16$. However, island ordering is observed only above a critical coverage somewhere between 0.15 and 0.25 ML. At $\theta = 0.2$ ML the average island width is 11 Å. If we use this value as a width of a single island in the limit of small coverage, the resulting L_0/D ratio becomes 0.28, which is within the predicted size ratio interval.

However this interpretation of the observed Cu island ordering is to be treated with some caution, since Eqs. (1) and (2) are strictly valid only for equilibrated systems. It has been noted that at $T_s = 300$ K, the Cu island shape is determined by the growth kinetics, e.g. by the limited mobility of adatoms. Hence we cannot exclude kinetic pathways which might also lead to semi-ordered island structures during growth [26].

3.2. $T_s \geq 400$ K, approaching thermodynamic growth conditions

Fig. 4 displays the growth of Cu on Pd(110) at $T_s = 400$ K. At this temperature, most of the deposited submonolayer Cu diffuses to substrate step

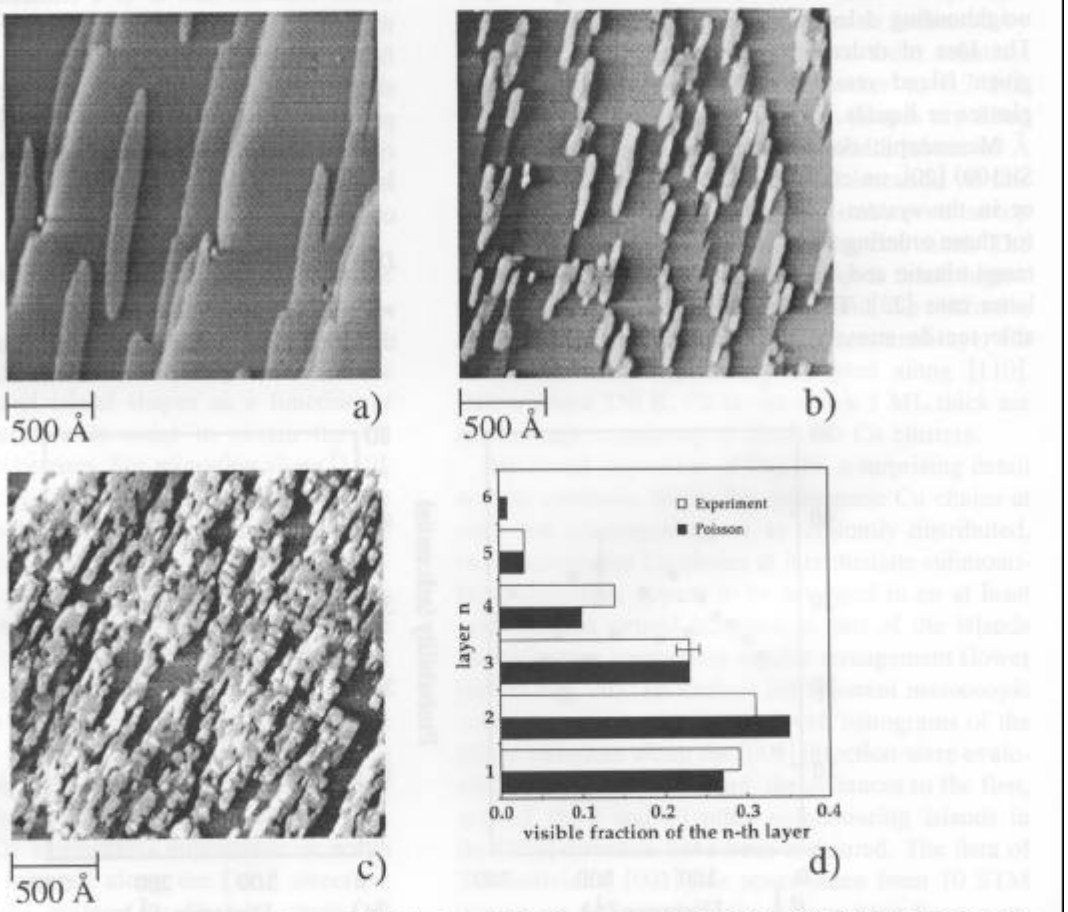

Fig. 4. Series of STM images showing the growth of Cu on Pd(110) at $T_s = 400$ K. Cu coverages (a) 0.45 ML, (b) 1.2 ML, (c) 2.3 ML. All images span the size 2100 Å × 2100 Å. (d) Histogram showing the visible fraction of the nth layer in image (c) and the corresponding Poisson law corresponding to an ideal three-dimensional Cu growth from the second layer on.

edges, as indicated by the "fingers" growing outward from steps. Thus narrow Pd terraces are wetted in a step flow mode. Isolated Cu islands are only formed on very large terraces (Fig. 4a). They are typically lens shaped and still elongated along [1$\bar{1}$0], the direction of "easy" diffusion. Second layer nucleation is only observed after the first pseudomorpic Cu layer is nearly completed (e.g. $\theta > 0.9$) (Fig. 4b). The film morphology of thicker films is still dominated by kinetics; Fig. 4c shows that at $T_s = 400$ K Cu growth proceeds via a *kinetic* Stranski–Krastanov mode. On the complete first monolayer, large three-dimensional Cu clusters develop, their edges being accurately oriented along the high symmetry directions of the substrate. For a perfect three-dimensional film growth (i.e. no interlayer mass transport) at $\theta > 1$, it is necessary that atoms aggregate on the same level on which they land. Then the visible fraction A_n of the layer n follows a Poisson law $A_n = (\theta^n/n!)\exp(-\theta)$ [27]. Fig. 4d shows the Poisson law for $\theta = 1.3$, since 3D growth begins only after the completion of the first monolayer in comparison with the corresponding STM data of Fig. 4c (Cu coverage 2.3 ML). The experimental data ressemble strongly the Poisson curve, however it is not excluded that some interlayer mass transport may have taken place.

When the deposition temperature approaches 600

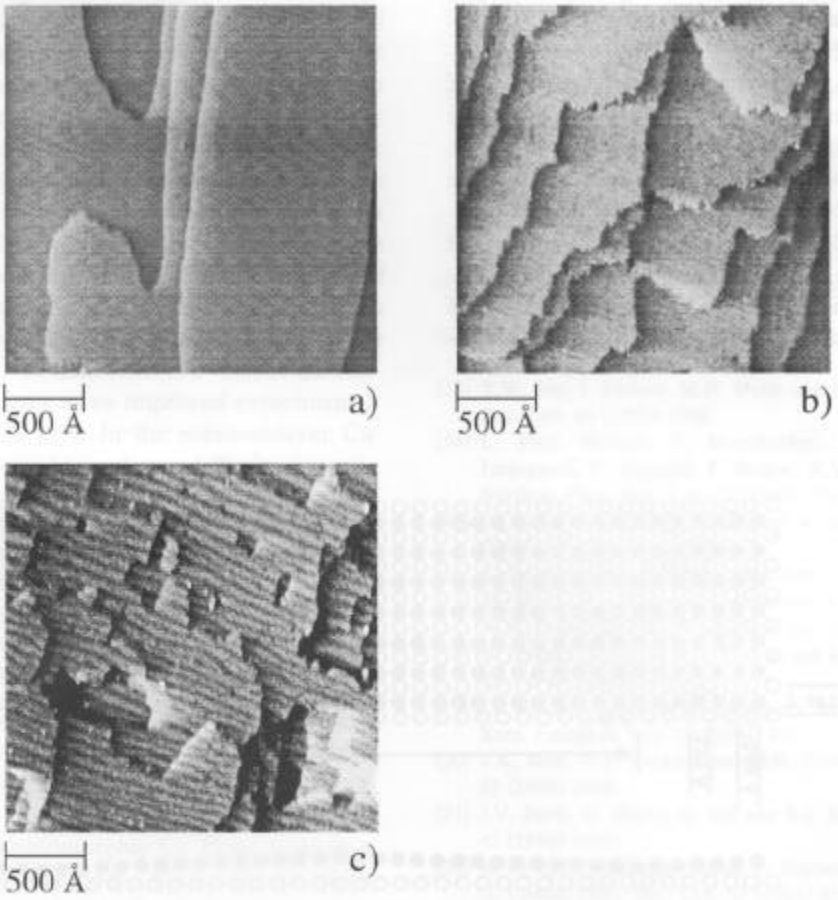

Fig. 5. Series of STM images showing the growth of Cu on Pd(110) at $T_s = 600$ K. Cu coverages (a) 1.1 ML, (b) 2.3 ML, (c) 10 ML. All images span the size 2400 Å × 2400 Å.

K, a transition from three- to two-dimensional Cu growth occurs (Fig. 5). In the submonolayer range, nucleation of isolated Cu islands is not observed anymore. Cu wets the substrate in a pure step-flow mode. At $T_s = 600$ K, this step-flow mode is maintained also in the Cu multilayer range (Fig. 5b), up to at least 10 ML. Up to a coverage of 5 ML the flat Cu films grow pseudomorphically on Pd(110), as evidenced by a sharp (1×1) LEED pattern and the flat imaging by STM. From a thermodynamic point of view, the growth of thick (1×1) Cu films is very improbable, since the total strain energy in the film (7% lattice misfit!) increases linearly with film thickness [28].

Indeed we observe above the critical coverage of 5 ML a partial strain relief of the tensile strain through buckling in the $[1\bar{1}0]$ direction. This relaxation is detected in the STM images as a striped pattern with the stripes running along [001] (Fig. 5c). The pattern corresponds to a buckling with a periodicity of 79 ± 1 Å, indicating an uniaxial reduction of the tensile strain to 4% along $[1\bar{1}0]$. The height variation from light to dark stripes is about 0.5 Å. Neither the periodicity nor the height modulation varies considerably when the Cu film thickness increases further. By LEED, the reconstruction was not detectable due to the limited resolution of our instrument (transfer-width < 200 Å). From the absence of any additional LEED spots and from the STM images it can however be concluded that the Cu atoms are still locked into their positions between the closed-packed atom rows of the underlying layer ([001] direction), but try to minimize strain by reducing the interatomic distances along the $[1\bar{1}0]$ direction.

Fig. 6 shows a possible model of the reconstructed Cu film surface at coverages above 5 ML. From the observed periodicity of 79 Å it can be calculated that the interatomic spacing along $[1\bar{1}0]$ is reduced to 2.66 Å. Thus from the 6th layer on, 30 Cu atoms are situated onto 29 atoms of the unreconstructed 5th layer (or the Pd substrate, respectively). Regions where Cu atoms occupy near bridge sites alternate with regions where atoms rest in near fourfold hollow sites, which explains the surface buckling. Obviously, maximum stress release cannot be achieved by reducing the interatomic distances along $[1\bar{1}0]$ to the Cu bulk value (2.55 Å). This may be due to the rigid atom positions in the perpendicular [001] direction, energetically preventing a further compression. The shown model is somewhat oversimplified since the system will try to minimize the occupation of energetically unfavorable bridge sites. In reality, more Cu atoms will be locked into fourfold hollow sites, whereas the atom density will be lower in the bridging regions. Finally it is noted that the density of dislocations (see Fig. 5c) increases with the film thickness, contributing additionally to the release of

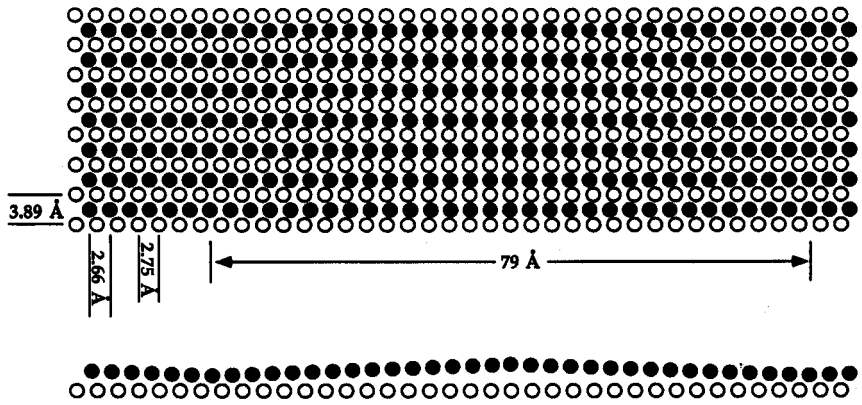

Fig. 6. Model of the uniaxial compression structure of thick Cu layers (here $\theta = 6$ ML) deposited at 600 K in top- and side-view. Full circles: Cu atoms in the 6th layer. Open circles: 5th layer Cu atoms.

stress in the Cu film. Both effects, the uniaxial compression and the dislocation formation, make it possible that Cu layer-by-layer growth continues up to 10 ML, despite the quite large lattice mismatch.

For deposition temperatures higher than 600 K, thin Cu films appear completely flat in STM images, which would mean that step-flow occurs also at high temperatures. RAIRS (reflection absorption infrared spectroscopy) measurements of CO adsorbed on high temperature deposited Cu films, however, give a completely different picture [29]. From these data it becomes evident that at about 750 K, CuPd surface alloy formation sets in. By STM, this phenomenon is not detectable since Cu and Pd atoms within the same layer do not give rise to any height contrast. Within the accuracy of the CO titration method ($< 5\%$ "foreign" atoms within the uppermost layer can be detected), CuPd intermixing can be excluded for temperatures lower than 750 K.

4. Conclusions

The growth of thin Cu films on Pd(110) has been studied by variable-temperature scanning tunneling microscopy. The study reveals the power of this imaging technique to study the growth mode and morphology of vapor-phase grown metal films on the atomic scale. In the present study the accessible temperature range was limited to 150–600 K but has been extended recently in an improved experimental set-up to 25–800 K [30]. In the submonolayer Cu range, the anisotropy of Cu adatom diffusion (migration barriers 0.51 eV along $[1\bar{1}0]$ and 0.75 eV along [001]) determines the Cu island shapes. In the extreme case of low deposition temperature ($T_s \leq 300$ K) and very low Cu coverage ($\theta < 0.1$ ML) monatomic Cu chains oriented along $[1\bar{1}0]$ are formed. In the Cu multilayer range, we find 4 different growth modes depending on T_s. At $T_s < 400$ K, microrough Cu films consisting of small 3D clusters are observed. Between 400 and about 550 K, a kinetic Stranski–Krastanov growth with a critical thickness of one monolayer takes place. Between 550 and 750 K, pseudomorphic Cu films grow in a layer-by-layer step-flow mode. Above 750 K, CuPd intermixing is observed. Despite the large misfit of 7% the Cu layers grow pseudomorphically up to 5 monolayers. This remarkable fact seems to point to rather small strain energies for copper under epitaxial strain. Films thicker than 5 ML partially relieve the tensile strain by uniaxial buckling into a high-order commensurate structure. In the relaxed structure the strain is homogeneously relieved over mesoscopic lengths. This is at variance with the strain relief picture evolving for fcc (111) heterointerfaces, where the lattice mismatch is locally relieved via the formation of networks of narrow domain walls [31].

References

[1] E. Bauer, Z. Kristallographie 110 (1958) 372.
[2] R. Kunkel, B. Poelsema, L.K. Verheij and G. Comsa, Phys. Rev. Lett. 65 (1990) 733.
[3] Z. Zhang and M.G. Lagally, Phys. Rev. Lett. 72 (1994) 693.
[4] S.C. Wang and G. Ehrlich, Phys. Rev. Lett. 67 (1991) 2509.
[5] C. Günther, S. Günther, E. Kopatzki, R.Q. Hwang, J. Schröder, J. Vrijmoeth and R.J. Behm, Ber. Bunsenges. Phys. Chem. 97 (1993) 522.
[6] J.H. Sinfelt, Bimetallic Catalysts (Wiley, New York, 1983).
[7] V. Ponec, Surf. Sci. 272 (1992) 111.
[8] K.I. Choi and M.A. Vannice, J. Catal. 131 (1991) 36.
[9] B. Oral, R. Kothari and R.W. Vook, J. Vac. Sci. Technol. A 7 (1989) 2020.
[10] H. Li, S.C. Wu, D. Tian, J. Quinn, Y.S. Li, F. Jona and P.M. Marcus, Phys. Rev. B 40 (1989) 5841; B 44 (1991) 8261.
[11] E. Kampshoff, E. Hahn, N. Wälchli and K. Kern, to be published.
[12] S. Rousset, S. Chiang, D.E. Fowler and D.D. Chambliss, Phys. Rev. Lett. 69 (1992) 3200.
[13] Y.W. Mo, J. Kleiner, M.B. Webb and M.G. Lagally, Phys. Rev. Lett. 66 (1991) 1998.
[14] L. Pleth Nielsen, F. Besenbacher, I. Stensgaard, E. Lægsgaard, C. Engdahl, P. Stoltze, K.W. Jacobsen and J. Nørskov, Phys. Rev. Lett. 71 (1993) 754.
[15] E. Hahn, A. Fricke, H. Röder and K. Kern, Surf. Sci. 297 (1993) 19.
[16] K. Besocke, Surf. Sci. 181 (1986) 145.
[17] M. Wolf, A. Goschnik, J. Lobova-Cackovic, M. Grunze, W.N. Unertl and J.H. Block, Surf. Sci. 182 (1987) 489.
[18] H. Hörnis, J.R. West, E.H. Conrad and R. Ellialtioglu, Phys. Rev. B 47 (1993) 13055.
[19] J.P. Bucher, E. Hahn, P. Fernandez, C. Massobrio and K. Kern, Europhys. Lett. 27 (1994) 473.
[20] F.K. Men, W.E. Packard and M.B. Webb, Phys. Rev. Lett. 61 (1988) 2469.
[21] J.V. Barth, H. Brune, G. Ertl and R.J. Behm, Phys. Rev. B 42 (1990) 9307.
[22] K. Kern, H. Niehus, A. Schatz, P. Zeppenfeld, J. Goerge and G. Comsa, Phys. Rev. Lett. 67 (1991) 855.
[23] D. Vanderbilt; in: Computations for the Nano-Scale, Eds. P.E. Blöchl et al. (Kluwer, New York 1993) p.1.

[24] V.I. Marchenko, JETP Lett. 55 (1992) 73.
[25] P. Zeppenfeld, M. Krzyzowski, C. Romainczyk, G. Comsa and M. Lagally, Phys. Rev. Lett. 72 (1994) 2737.
[26] A. Wheeler, C. Ratsch, A. Morales, H. Cox and A. Zangwill, Phys. Rev. B 46 (1992) 2428.
[27] M. Bott, T. Michely and G. Comsa, Surf. Sci. 272 (1992) 161.
[28] J.G. Dash, J. Vac. Sci. Technol. A 5, (1986) 1523.
[29] E. Hahn, E. Kampshoff, and K. Kern, Chem. Phys. Lett. 223 (1994) 347, and to be published.
[30] H. Brune, H. Röder and K. Kern, Appl. Phys. A, (1994), in press;
see also H. Röder, E. Hahn, H. Brune, J.P. Bucher and K. Kern, Nature 366 (1993) 141.
[31] H. Brune, H. Röder, C. Boragno and K. Kern, Phys. Rev. B 49, (1994) 2997.